| | |
|---|---|
| Title | Evaluating the interaction of human serum albumin (HSA) and 1,2-dimyristoyl-sn-glycero-3-phosphocholine (DMPC) liposomes in different aqueous environments using anisotropy resolved multi-dimensional emission spectroscopy (ARMES) |
| Author(s) | Gordon, Fiona; Casamayou-Boucau, Yannick; Ryder, Alan G. |
| Publication Date | 2022-01-07 |
| Publication Information | Gordon, Fiona, Casamayou-Boucau, Yannick, & Ryder, Alan G. (2022). Evaluating the interaction of human serum albumin (HSA) and 1,2-dimyristoyl-sn-glycero-3-phosphocholine (DMPC) liposomes in different aqueous environments using anisotropy resolved multi-dimensional emission spectroscopy (ARMES). Colloids and Surfaces B: Biointerfaces, 211, 112310. doi:https://doi.org/10.1016/j.colsurfb.2021.112310 |
| Publisher | Elsevier |
| Link to publisher's version | https://doi.org/10.1016/j.colsurfb.2021.112310 |
| Item record | http://hdl.handle.net/10379/17309 |
| DOI | http://dx.doi.org/10.1016/j.colsurfb.2021.112310 |

Colloids and Surfaces B: Biointerfaces 211 (2022) 112310

Contents lists available at ScienceDirect

Colloids and Surfaces B: Biointerfaces

journal homepage: www.elsevier.com/locate/colsurfb

# Evaluating the interaction of human serum albumin (HSA) and 1,2-dimyristoyl-*sn*-glycero-3-phosphocholine (DMPC) liposomes in different aqueous environments using anisotropy resolved multi-dimensional emission spectroscopy (ARMES)

Fiona Gordon, Yannick Casamayou-Boucau, Alan G. Ryder *

*Nanoscale BioPhotonics Laboratory, School of Chemistry, National University of Ireland, Galway, Galway H91 CF50, Ireland*

ARTICLE INFO

*Keywords:*
Fluorescence
Proteins
Liposome
Chemometrics
Anisotropy
Modeling

ABSTRACT

Studying the interaction between plasma proteins and liposomes is critical, particularly for their use as drug delivery systems. Here, the efficacy of anisotropy resolved multidimensional emission spectroscopy (ARMES) for investigating the interaction of human serum albumin (HSA) with liposomes was explored and compared to conventional spectroscopic techniques. Dynamic Light Scattering (DLS) and absorbance spectroscopy (with Multivariate Curve Resolution (MCR) modeling) indicated that the highest degree of liposome rupturing, and aggregation occurred in water, with less in ammonium bicarbonate buffer (ABC) and phosphate buffered saline (PBS). Fluorescence emission spectra of HSA-liposome mixtures revealed significant hypsochromic shifts for water and ABC, but much less in PBS, where the data suggests a non-penetrating protein layer was formed. Average fluorescence lifetimes decreased upon liposome interaction in water (6.2→5.2 ns) and ABC buffer (6.3→5.6 ns) but increased slightly for PBS (5.6→5.8 ns). ARMES using polarized Total Synchronous Fluorescence Scan measurements with parallel factor (PARAFAC) analysis resolved intrinsic HSA fluorescence into two components for interactions in water and ABC buffer, but only one component for PBS. These components, in water and ABC buffer, corresponded to two different HSA populations, one blue-shifted and penetrating the liposomes ($\lambda_{ex/em}$ = ~ 280/320 nm) and a second, similar to free HSA in solution ($\lambda_{ex/em}$ = ~ 282/356 nm). PARAFAC scores for water and ABC buffer suggested that a large proportion of HSA interacted in an end on configuration. ARMES provides a new way for investigating protein-liposome interactions that exploits the full intrinsic emission space of the protein and thus avoids the use of extrinsic labels. The use of multivariate data analysis provided a comprehensive and structured framework to extract a variety of useful information (resolving different fluorescent species, quantifying their signal contribution, and extracting light scatter signals) all of which can be used to discriminate between interaction mechanisms.

## 1. Introduction

Liposomes are spherical vesicles containing at least one lipid bilayer, typically 50–500 nm in diameter, which spontaneously form when certain lipids are hydrated with aqueous media [1]. Since the 1960's [2] liposomes have found multiple uses [3], being used as models for membranes and simple cells, allowing in vitro investigation of a broad range of biochemical processes [4,5]. Liposomes are also used as drug delivery systems (DDS) [6–8], being able to modulate pharmacokinetics and pharmacodynamics of entrapped drugs by protecting them against chemical and immunological breakdown, thereby reducing unwanted side-effects [9]. In the context of their use in vivo, it is important to characterize the interaction of liposomes with serum constituents, particularly proteins [10,11].

Interaction of liposomes with plasma proteins can dramatically affect stability and in vivo behavior which in turn impacts on DDS efficacy [12–15]. An important factor to consider when studying protein-liposome interactions (particularly when using in-vitro model systems) is the aqueous environment in which the interaction takes place. The aqueous environment (e.g., pH and ionic strength) changes physicochemical properties of both protein and liposome and will therefore influence the interaction [16,17]. Some studies avoid the use

* Corresponding author.
*E-mail address:* alan.ryder@nuigalway.ie (A.G. Ryder).

https://doi.org/10.1016/j.colsurfb.2021.112310
Received 10 August 2021; Received in revised form 9 December 2021; Accepted 26 December 2021
Available online 29 December 2021

of buffers, using water instead to promote interaction [10,11]. However, in order to better replicate physiological conditions buffers are required [18], primarily to prevent protein aggregation [19,20], but the composition and ionic strength of buffers also affects liposome properties like size and membrane rigidity [21,22]. For example, the interaction of a zwitterionic liposome, POPC, and magainin, with different salt concentrations, showed a decrease in interaction with increasing salt concentration. The decreased interaction is caused by a combination of factors including increased membrane rigidity along with protein stabilization at high salt concentration, which reduces the propensity for interaction [21,22]. Conversely in low ionic strength solutions, like water, the protein is less stable making interactions between hydrophobic regions of the proteins and the zwitterionic lipid bilayer more energetically favorable [23].

Protein–liposome interactions are often studied using conventional 2D fluorescence measurements of intrinsic protein emission [24–26]. However, intrinsic protein fluorescence contains overlapping Tyr and Trp emission leading to complex emission spectra. This overlap limits the information available from 2-D spectra, so multi-dimensional fluorescence (MDF) measurements are preferred as this can facilitate spectral resolution into the constituent fluorophores. MDF spectra can be collected either as Excitation Emission Matrices (EEM) or as total synchronous fluorescent scans (TSFS) [27, 28]. In situations where significant particles are present, producing high degrees of light scatter, such as for bioprocess broth analysis [29], or liposome analysis, TSFS measurements are preferred.

MDF spectroscopy can be further enhanced by adding anisotropy (or polarization) information making a 4D measurement. Using polarized EEM (pEEM) and polarized TSFS (pTSFS) measurements provides a new approach for studying complex systems containing proteins [30–34]. This measurement methodology has been further developed into anisotropy resolved multidimensional emission spectroscopy (ARMES) [35,36] which combines multivariate data analysis methods like Parallel Factor (PARAFAC) or Multivariate Curve Resolution (MCR) to specifically resolve individual fluorophore contributions from complex spectra [32,37]. PARAFAC is the most popular method for resolving MDF spectra [38,39], and here it is used for analyzing the changing intrinsic HSA emission during interaction with DMPC (dimyristoyl-*sn*-phosphatidylcholine) liposomes.

Here, we explore the efficacy of pTSFS measurements and ARMES data analysis for studying protein-liposome interactions and compare the information obtained with that obtained from conventional absorbance, fluorescence steady-state, and lifetime spectroscopies, and Dynamic Light Scattering (DLS) measurements. DMPC is neutrally charged and easily forms liposomes, and we used HSA in different buffers as a model to investigate protein–liposome interactions (Fig. S1, SI). DMPC liposomes of ~ 200 nm diameter were used for two reasons: first because they are stable in water and buffer, and second because they are also used for DDS [40,41]. HSA was selected as it is the major serum protein present in blood and is a relatively simple protein in terms of structure and fluorescence. HSA has a heart like shape [42] 3.8 × 15 nm in size [43,44], with three domains each of which contains two subdomains [45]. Intrinsic HSA fluorescence is dominated by the single tryptophan fluorophore (Trp-214), with a smaller contribution from 17 tyrosine residues, while the phenylalanine contribution is negligible [46]. Liposomes were also labeled with a FRET pair of lipophilic dyes: 1,1'-Dioctadecyl-3,3,3',3'-Tetramethylindocarbocyanine perchlorate (Dil) and 1,1'-Dioctadecyl-3,3,3',3'-Tetramethylindocarbocyanine, 4-Chloro--benzenesulfonate salt (DiD) to provide a FRET based extrinsic fluorescence method for monitoring protein-liposome interactions [47,48].

## 2. Materials and methods

### 2.1. Materials

1,2-dimyristoyl-*sn*-glycero-3-phosphocholine (DMPC) (850345P-1G, Lot no. 274) was purchased from Avanti polar Lipids. 1,1'-Diooctadecyl-3,3,3',3'-Tetramthylindocarbocyanine Perchlorate (Dil) (D282, lot no. 2095333) and 1,1'-Diooctadecyl-3,3,3′,3′-Tetramthylindocarbocyanine, 4-Chlorobenzenesulfonate Salt (DiD) (D7757, lot no. 2071577) lipophilic dyes were purchased from Sigma Aldrich. Chromasolv® water (772-18-5, lot no. BCCD42850) was purchased from Fisher Chemicals. Phosphate buffered saline, PBS, (P4417) tablets were purchased from Fisher Chemicals and used to make a 10 mM buffer solution of pH ~7.4. $NH_4HCO_3$ was purchased from Fisher and used to make a 50 mM buffer solution of pH ~7.8. HSA (A1887, lot no. SLMBM7779V) was purchased from Sigma Aldrich and used without further purification. Chloroform (99%+, Extra Pure) and ethanol (99%+, Absolute, Extra Pure) were also purchased from Fisher Chemicals. All materials were used as received.

### 2.2. Sample preparation

Stock solutions (1 mM) of lipophilic dyes (Dil and DiD) were prepared in ethanol [47,48]. Mixtures of lipids (10 mg/ml) and lipophilic dyes (< 0.5% labeling ratio) were homogenously dispersed in chloroform and dried overnight under vacuum. The resulting lipid thin film was re-suspended in water or buffer. Large unilamellar vesicles were prepared via extrusion using an Avanti mini-extruded kit with a heating block at 25°C, above the phase transition temperature of DMPC, using 200 nm polycarbonate filters (Whatman, 800281). Liposomes were freshly prepared daily and analyzed within 8 hours. Nine separate extrusions were made for every sample mixture with 3 replicate samples prepared in each of the water, PBS, and ABC buffers. The number of lipids per liposome, was estimated using the Mozafari *et al.* method (Eqs. (S1) & (S2), Table S1, SI) [49].

To prepare protein-liposome samples, stock solutions of HSA (4 mg/ml, 0.2 μm filtered) and extruded DMPC liposomes (5 mg/ml) were prepared in water, PBS, and ABC buffers. Ten different mixtures were prepared with a constant DMPC concentration (0.25 mg/ml, 0.37 mM) and varying HSA concentrations (0–2 mg/ml, 0–0.03 mM), corresponding to 1:185–1:12 HSA:DMPC molar ratios. All samples were incubated at 25 °C for ~2–3 h prior to analysis to ensure complete interaction between protein and liposome.

### 2.3. Spectroscopy

DLS measurements were collected at 25 °C using a Zetasizer® Nano ZS (*Malvern Panalytical Ltd.*) after samples being first equilibrated at 25 °C for 120 s (see Section 1.2, SI for more details). DLS analysis was conducted using the Zetasizer software ver. 7.13 (*Malvern Panalytical Ltd.*). UV–visible absorbance spectra at 25 °C were obtained from samples pipetted into semi-micro quartz cuvettes (10 × 4 mm) (*Light-path Optical Ltd UK*) using Cary 60 spectrophotometer (*Agilent Technologies*) along the short axis of the cuvette.

Steady-state emission and pTSFS spectra were collected at 25 °C with a Cary Eclipse Spectrophotometer (*Agilent Technologies*) fitted with wire-grid polarizers (Fig. S2, SI) [35] with samples held in semi-micro quartz cuvettes (10 × 4 mm). Excitation was along the short axis (4 mm) and emission was collected along the long axis (10 mm). pTSFS spectra were collected (see Section 1.2 in SI for a more detailed explanation of measurements and ARMES) over a 250–310 nm excitation range with varying wavelength offsets of 20–150 nm (corresponding to $\lambda_{em}$ = 270–400 nm) with 2 nm step increments for both axes and the scan rate was 1200 nm $min^{-1}$ with PMT voltage of 875 V. Wavelength offsets of $\Delta\lambda \geq 20$ nm [33] were used, to minimize the Rayleigh scattering contamination. Three different 2D emission scans were also collected measuring HSA emission ($\lambda_{ex/em}$ = 280/310–420 nm) and two regions of the lipophilic dye's emission ($\lambda_{ex/em}$ = 532/550–700 nm (FRET trace) & $\lambda_{ex/em}$ = 620/640–740 nm (direct FRET acceptor excitation)), all spectra were collected with 1 nm increments, at 600 nm $min^{-1}$, and the photomultiplier tube detector (PMT) voltage of 875 V (for $\lambda_{ex}$ = 280 nm), 900 V (for $\lambda_{ex}$ = 532 nm), and 800 V (for $\lambda_{ex}$ = 620 nm). Excitation and

emission monochromator slit widths were 5 nm for all measurements.

All fluorescence emission measurements were collected using two different polarizer settings: VV (vertical-vertical), VH (vertical-horizontal). The instrumental G-factor was calculated each day from the HH (horizontal-horizontal), HV (horizontal-vertical) spectra of samples with the best SNR (the HSA only solutions). Anisotropy ($r$) was calculated using the standard formula [46,50] (see SI, Equations S3/S4). Magic-angle fluorescence decays were recorded using a Time Correlated Single Photon Counting system, Fluotime 200 (*PicoQuant GmbH, Berlin*). Excitation was a 295 nm 4 MHz pulsed LED (PLS-8-2-299, *PicoQuant*) and emission was collected at 350 nm with a 35 ps time resolution. Decays were collected to 20,000 counts in the peak channel. Instrument response function was measured using a diluted (1:1000) Ludox solution. Lifetimes were calculated by iterative reconvolution using the FluoFit software ver. 4.6.6 (*PicoQuant*). A tri-exponential model was required, and the fits were considered appropriate once $\chi^2$ reached values < 1.25, and residuals did not show systematic trends (Fig. S8, SI). Here we used the intensity weighted average lifetime (Equation S5, Table S2, SI).

### 2.4. Data analysis

Data analysis of 2-D spectral data and multidimensional ARMES spectral data was conducted using PLS toolbox ver. 8.2.1 (*Eigenvector Research Inc.*), MATLAB ver. 9.1.0 (*The Mathworks Inc.*) and in-house codes. UV-Vis absorbance spectra were analyzed by MCR-ALS [51] in order to resolve HSA absorbance from the light scatter signal of the DMPC liposomes, and get accurate relative contributions (see SI for more details). The data matrix **D** (108 × 76) was constructed with 108 rows representing the absorbance spectra in all buffers of the different HSA-liposome mixtures, and the DMPC and HSA stock solutions, all measured in triplicate. The columns (n = 76) were the absorbance values, measured at 1 nm intervals between 250 and 400 nm. Non-negativity constraints were set in both spectral and concentration modes. One-component in the spectral mode was fixed (equality constraint) to the absorbance spectrum of pure HSA spectra (Section 1.5, SI). Fixing this one component only marginally increased the lack of fit (Table S3, SI), but it enabled better modeling of the HSA signal at lower concentrations, and also removed rotational ambiguities compared to only using non-negativity constraints (Tables S4/S5, SI).

For 2D and 3D MDF fluorescence spectra, HH and HV polarization spectra were used to calculate the G-factor ($G = I_{HV}/I_{HH}$). This was used to correct VH spectra for polarization bias, giving the corrected perpendicular $S/TSFS_{\perp}$ spectra. VV polarization spectra are the parallel polarized, $S/TSFS_{\parallel}$, spectra. Total unpolarized $S/TSFS_T$ spectra were calculated from the parallel and perpendicular spectra as follows: $S/TSFS_T = S/TSFS_{\parallel} + (2 \times S/TSFS_{\perp})$. Raman scattering was reduced by blank subtraction of a buffer spectrum from sample spectra. Spectra were Savitzky-Golay smoothed to reduce unwanted noise, inner filter effect (IFE) [52] correction was not implemented due to strong liposome light scattering and relatively high protein concentrations used. When using TSFS, it is secondary IFE (i.e., scattering of the protein emission by the liposomes) which is a significant contributor to emission signal changes.

Changes in TSFS raw spectra (only corrected with water/buffer and G-factor for VH data) caused by interaction with the liposomes were first explored using PCA analysis [53]. Prior to PCA, the global dataset containing all samples was re-shaped to form a two-way dataset (108 × 2046 (interaction samples n = 90, stock DMPC liposomes n = 9, stock HSA n = 9)), and mean centering was applied before modeling. Before PARAFAC analysis [54–56], TSFS spectra were transformed to a trilinear EEM layout, and designated: $t\text{-}EEM_T$, $t\text{-}EEM_{\perp}$, and $t\text{-}EEM_{\parallel}$ [57]. For PARAFAC the liposome only spectrum in either water, ABC or PBS buffer was subtracted to try and reduce excitation light scatter artefacts. For t-EEM data, interpolation was used to accommodate areas with no experimentally acquired spectral information [33]. Then the data was cut down to select the area of interest ($\lambda_{ex/em}$ = 250–310 / 270–400 nm). Pre-processed t-EEM data were arranged in a three-way array (**X**) of size 99 × 66 × 31 and 33 × 66 × 31 (samples×$\lambda_{em}$×$\lambda_{ex}$) for global (all samples, all buffers) and sub-models (per interaction medium), respectively (where interaction samples n = 90/30, stock HSA n = 9/3).

## 3. Results and discussion

The HSA and liposome only solutions, were first characterized using conventional analytical methods to determine size, stability, and quality. Then the HSA-liposome mixtures were examined first by conventional techniques, and then by the more complex pTSFS measurements, multivariate data analysis, and the ARMES method. The goal being to see what additional information about protein-liposome interactions can be extracted by pTSFS and ARMES. A diagram showing the data analysis scheme for the spectroscopic measurements and the outputs is provided in Fig. S3, SI.

### 3.1. DLS analysis

DLS analysis of the freshly extruded liposome solutions over 48 h (Fig. S4, SI) was used to validate that successful extrusion had been achieved [58,59] and to assess if they were stable over the timeframes used for protein-liposome interaction experiments. Small size changes (< 4%) were detected in all cases, indicating the liposomes were sufficiently stable for 8-hours, and thus observed changes should be caused by interaction with protein. The liposomes had relatively low PDI (< 0.2) in all solutions [60], with average hydrodynamic diameters of 137.8, 161.6, and 166.3 nm in water, ABC buffer, and PBS, respectively (Table 1, Fig. S5, SI). Liposomes were smallest in water because zwitterionic lipid vesicles are known to swell in salt solutions [61]. This swelling is thought to be primarily driven by weakening of van der Waals (vdW) attraction between lipids and solvent, the strength of this interaction is proportional to the dielectric constant difference between lipid and solvent, the larger the difference, the stronger the attraction between adjacent bilayers [62].

DLS revealed that HSA hydrodynamic diameter increased very significantly from 7.8 nm in water, to 9.5 and 9.6 nm in PBS and ABC buffer buffers respectively (Table 1 & Fig. S6, SI). This size difference was due to electrostatic stabilization of the protein structure into a larger extended ellipsoid or oblate ellipsoid conformation by counterions present in the buffers. Conversely in water, HSA is more compact because due to the lack of pH buffering capacity and counterions in solution necessary to increase the proteins conformational stability through electrostatic stabilization [20,63]. DLS also revealed a higher PDI (and lower peak 1 contribution) in water which suggests the presence of more aggregates (Table 1) [64,65]. These structural and composition differences will have a significant impact on the interaction with liposomes. After incubation with HSA, the liposomes were extensively ruptured in water, with DLS measurements not being reproducible but indicating multiple size populations (Fig. 1G) making quantitative analysis impossible [66,67]. However, in ABC and PBS buffers, liposomes appeared much more stable, and DLS showed that there were two size populations of particles. For liposomes incubated with 2 mg/ml HSA, in ABC and PBS buffers, polydispersity increased to ~ 0.24 and ~ 0.29, and average particle size increased to ~ 170 and ~ 215 nm respectively. The bimodal distribution in the volume data showed peaks at ~ 150–200 nm and at ~ 250–350 nm (Fig. 1H and I, Fig. S7, SI). The first population is related to a combination of both free, unperturbed liposome (if any remained in solution) and liposomes with protein coatings. The second population was probably due to aggregates of the protein-liposome species [68]. Studies have reported that protein monolayer (or protein corona) formation on liposome surfaces can make the surface more adhesive, thus inducing formation of large particle clusters which seems to be the case here [69,70].

**Table 1**
(top-half of table): Average particle size (Z-average, nm), approximate number of lipid molecules per liposome, and surface area per liposome (calculated from Z-average), peak 1 size (nm), polydispersity index (PDI), and percentage area calculated from scatter intensity of peak 1 (%) of samples containing liposomes only; (middle) Size and surface area data and maximum number of HSA per liposome monolayer (calculated from surface areas), for HSA only samples; (bottom) Size data for liposome samples incubated with 2 mg/ml HSA in water, ABC buffer, and PBS.

| | Water | ABC | PBS |
|---|---|---|---|
| Liposome only samples: | | | |
| Z-average (diameter, nm) | 137.8 (± 1.4) | 161.6 (± 3.0) | 166.3 (± 1.5) |
| Liposome surface area ($nm^2$) | ~ 59,625 | ~ 82,041 | ~ 86,882 |
| Approx. no. lipids per liposome [49] | ~ 156,210 | ~ 217,132 | ~ 230,347 |
| Peak 1,diameter (nm) | 162.1 (± 2.7) | 188.6 (± 5.8) | 197.8 (± 2.1) |
| Polydispersity index | 0.11 (± 0.01) | 0.11 (± 0.02) | 0.13 (± 0.03) |
| Peak 1 (% area) | 100.0 (± 0.0) | 100.0 (± 0.0) | 100.0 (± 0.0) |
| HSA only samples: | | | |
| Z-average (diameter) (nm) | 7.8 ( ± 0.9) | 9.6 ( ± 0.5) | 9.5 ( ± 0.2) |
| HSA Surface area, circular area model from z-avg ($\pi r^2$), $nm^2$ | ~ 47.8 | ~ 72.4 | ~ 70.9 |
| Surface area per HSA, side on, $nm^2$. | ~ 44.8 | ~ 44.8 | ~ 44.8 |
| Surface area per HSA, end on, $nm^2$. | ~ 14.4 | ~ 14.4 | ~ 14.4 |
| Max no. HSA per monolayer (~circular area model) | ~ 1247 | ~ 1133 | ~ 1225 |
| Max no. HSA per monolayer (side-on) | ~1333 | ~ 1833 | ~ 1942 |
| Max no. HSA per monolayer (end-on)) | ~4141 | ~ 5697 | ~ 5995 |
| Peak 1 (diameter) (nm) | 5.8 (± 0.41) | 9.5 (± 0.19) | 9.8 (± 0.2) |
| Polydispersity index | 0.32 (± 0.05) | 0.25 (± 0.02) | 0.26 (± 0.02) |
| Peak 1 (% area) | 73.9 (± 1.0) | 87.8 (± 3.6) | 90.2 (± 1.9) |
| HSA/Liposome complexes (2 mg/ml): | | | |
| Z-average (nm) | 2983 (± 4077) Not reliable | 170.0 (± 40.3) | 214.5 (± 75.6) |
| Peak 1 (nm) | 137 (± 90) Not reliable / | 233.3 (± 80.1) | 258.1 (± 105.1) |
| Polydispersity index | 0.65 (± 0.32) Not reliable | 0.24 (± 0.08) | 0.29 (± 0.05) |
| Peak 1 (% area) | 91.6 (± 7.3) Not reliable | 100.0 (± 0.0) | 100.0 (± 0.0) |

### 3.2. Absorbance spectroscopy

Absorbance spectra of HSA-DMPC liposomes were analyzed using MCR-ALS to extract the concentration and pure absorbance and scattered light spectra. The MCR model (Fig. 2) on the global dataset (n = 108) is presented here, with specific buffer models included in the SI (Fig. S9, Table S3). Two components were extracted corresponding to: DMPC (mostly scattered light) and HSA explaining > 99.8% of the total variance, the HSA component accounted for 20.6% of the variance with DMPC accounting for 79.2% showing the significant impact that light scattered from the particles had on the measured spectra. For particles in the 150–200 nm range of this composition, and the wavelengths of light involved, the light scatter becomes much less isotropic and Mie scatter in the forward direction starts to dominate, particularly for parallel polarized light. Furthermore, the scatter component scores were much greater in water (Fig. 2B) which was expected with the larger degree of rupturing. For ABC and PBS buffers the scatter signal was nearly constant for all HSA additions which indicated a relatively stable particle size and distribution, which agrees with the DLS data. The recovered HSA scores were linear with increasing concentration in all cases which agreed with the Beer-Lambert law. Thus, MCR accurately resolved DMPC (i.e. the scttered light) and HSA (absorbance) contributions. However, this also shows the limitations of absorbance spectroscopy as there was no evidence for any spectral changes in either component thus, we cannot monitor the protein-liposome interaction apart from saying that in water the liposomes were highly disrupted by HSA. Thus, a more sensitive measurement method is needed.

### 3.3. 2D fluorescence emission and anisotropy analysis

The interaction between HSA and DMPC liposomes (Fig. 3A–B) resulted in significant blue-shifts of 22 and 17 nm for water and ABC buffer respectively ([HSA] = 0.13 mg/ml in t-EEM$_{\perp}$) [46]. In PBS under the same conditions, however, there was far less significant blue-shift of ~ 1 nm (Fig. 3C). Lifetime measurements of HSA emission showed a significant decrease upon interaction with DMPC liposomes in water and ABC buffer, but an increase in PBS (Fig. 4A–C, Table S2, SI). Unfortunately, conventional anisotropy measurements (Fig. 3D–F) were not useful or descriptive because of three factors: the significant amounts of free HSA in solution, spectral changes in HSA emission, and scattered light induced IFE.

These differences were due to different interaction mechanisms (unstable disruption for water, surface binding and penetration for ABC buffer, and non penetrating protein layer formation for PBS) modulated by the different ionic compositions. Simple geometrical calculations (Table 1), ignoring packing constraints, and structural changes in protein and liposome, indicate that between 1000 and 8000 HSA molecules are required to form a complete monolayer (Table S1, SI). This depended on whether HSA binds end-on, or side-on [71], or as a combination of both. HSA:liposome ratios were always > 800:1 and this, along with DLS measurements which showed size increases, suggested that we obtained protein layers in buffers but likely with incomplete coverage [10,72]. For PBS, where HSA was not observed to penetrate the bilayer, the increase in size was ~ 48 nm ($\Delta Z_{avg}$) which was more than twice that expected for a liposome with a uniform HSA monolayer. The larger than expected increase in size and polydispersity was probably due to the formation of larger protein-liposome aggregates [73]. Since neither emission nor lifetime changes very significantly in PBS we suggest that HSA appears to remain more in an aqueous like phase, lying flat on the particle surface rather than penetrating the lipid bilayer [74].

The blue-shifted HSA emission (and PARAFAC scores, *vide infra*) with DMPC in water and ABC buffer, suggested that for a significant population of HSA molecules the Trp-214 fluorophore was now located in a more hydrophobic environment. This might mean that for the liposomes in water and ABC buffer that HSA had penetrated the bilayer (and possibly undergone some degree of structural change), changing the local environment sufficiently to affect emission [75,76]. In ABC buffer, Z-average increased by ~ 9 nm which was compatible with slight swelling of the membrane caused by penetration. A uniform, non-penetrating monolayer should result in an increase of ~ 18 nm. It was likely that there were multiple types of particle present (as seen by DLS) which would include liposomes with protein coatings, that could contain both penetrating and non-penetrating proteins, and also larger liposomes/liposome-protein aggregates. Finally, in water where there was extensive disruption and a wide distribution of particle sizes generated, we also observed significant, blue-shifted emission caused by a changed HSA environment. The penetration and disruption of liposomes in water by HSA is supported by previous findings in which HSA was reported to coat the surface, penetrate [77–79], and deform the lipid bilayer [10,80,81]. The exact nature of the HSA-lipid/liposome complexes or aggregates requires further investigation, which necessitates the use of tools to measure the population distribution of the samples which is not feasible with DLS.

2D spectra and anisotropy of DiI and DiD emission, collected from samples after incubation, showed very little change with protein concentration (Fig. S10/S11). For ruptured vesicles which do not reform, lower FRET efficiencies should be observed, as was observed when liposomes were solubilized by detergents [47,48]. For PBS, all evidence

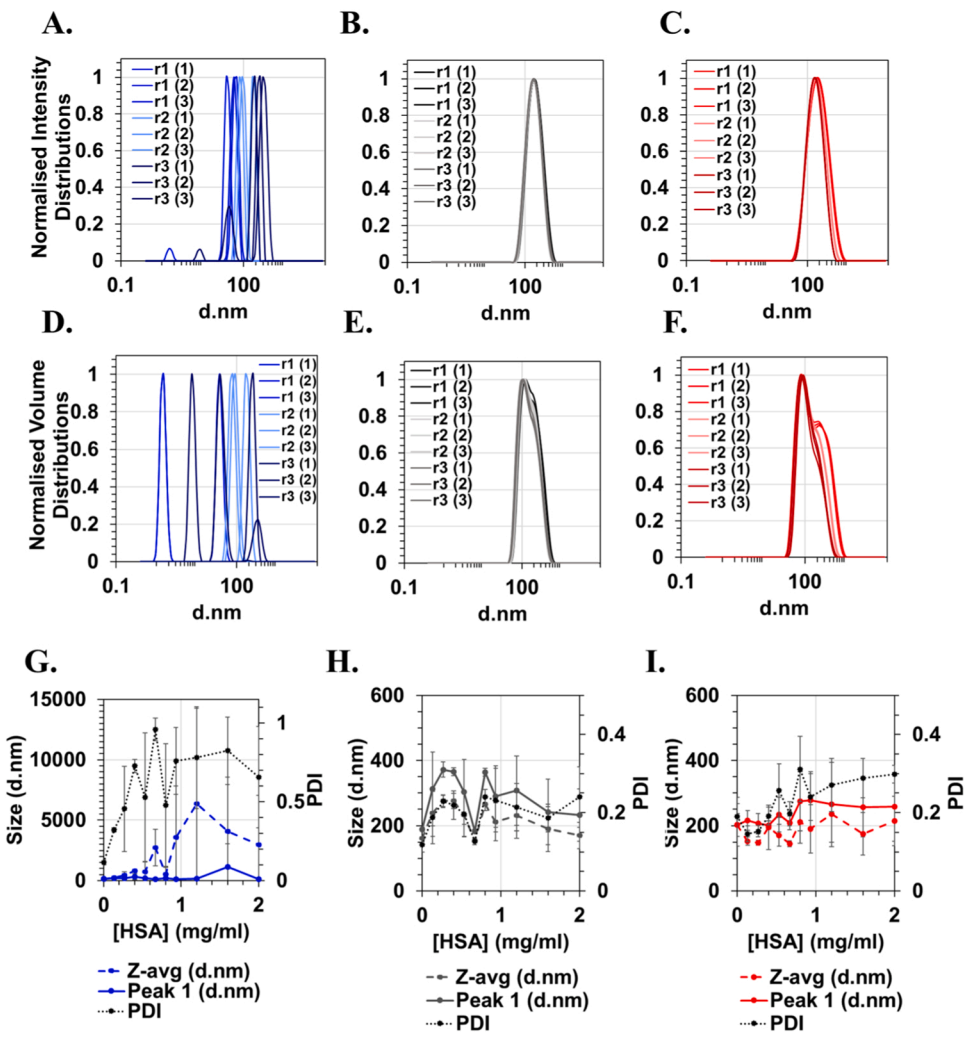


**Fig. 1.** DLS measurements of HSA-liposome mixtures. (A–C), DLS intensity based DLS distributions for 0.13 mg/ml HSA with liposomes in water (blue), ABC buffer (grey), and PBS (red)). (D–F), DLS volume based DLS distributions for the same samples in water (blue), ABC buffer (grey), and PBS (red)). (G and H), Changes in average particle size (Z-avg.), peak 1, and PDI of liposomes after addition of varying concentrations of HSA (0–2 mg/ml). See SI for DLS spectra of the liposome only (Fig. S5) and HSA (Fig. S6) only control samples.

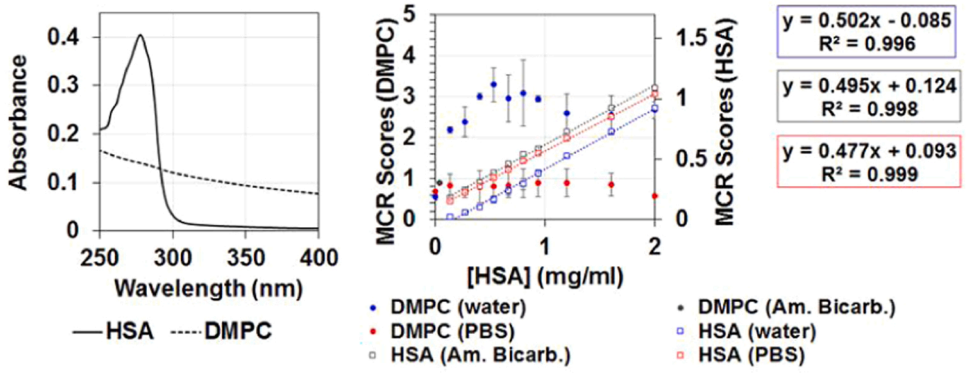


**Fig. 2.** MCR resolution of absorbance spectra from HSA-liposome mixtures showing: (A) The two components used which correspond to HSA absorbance (with some residual scatter at longer wavelengths) and light scattered from the DMPC liposomes, and: (B) The corresponding recovered MCR scores of these components in water, ABC, and PBS buffers, with HSA absorption showing a linear behavior with increasing concentration.

points to formation of a non-penetrating protein layer, with an unperturbed lipid bilayer, and no FRET change is expected or observed. For water, this, and other results, suggest that liposomes ruptured and reformed over the ~3-hour incubation time, whereas for ABC buffer, bilayer penetration was insufficient to cause significant disruption and thus change FRET [13,82]. As previously observed [34], calculated FRET efficiencies (Fig. S12) were higher for perpendicularly polarized measurements, which can be due to a combination of higher sensitivity to the depolarized emission arising from the indirect excitation via FRET, minimization of residual light scatter contamination, and reduced secondary IFE from emission scatter. Overall, the use of the Dil/DiD extrinsic fluorophores did not provide much useful information about protein-liposome interactions here.

Generally the insertion of Trp fluorophores into a more hydrophobic

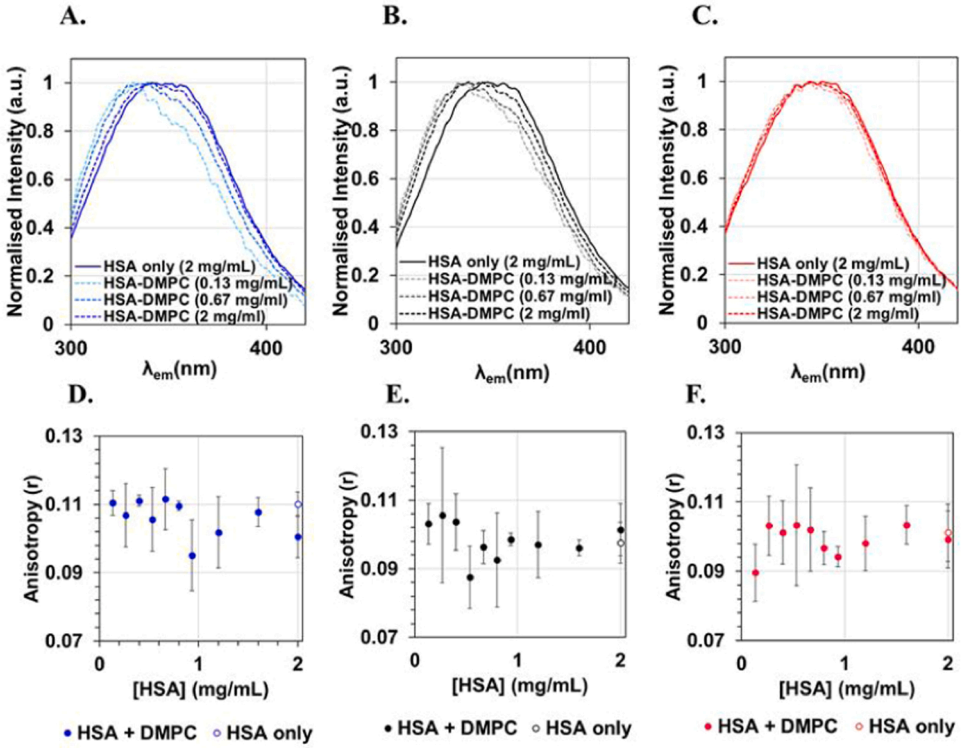


**Fig. 3.** (A–C): Fluorescence emission spectra of HSA ($\lambda_{ex}$ 280 nm) extracted from the t-EEM$_T$ data in: (A) Water, (B) ABC buffer, and (C) PBS, in the absence of liposomes (solid lines) and in the presence DMPC liposomes (dashed lines, showing largest shift at the lowest HSA concentration). (D–F): Anisotropy of HSA ($\lambda_{ex/em}$ 280/350 nm) in absence (unfilled circles) and presence of DMPC liposomes (filled circles) at increasing concentrations of HSA in: (D) Water, (E) ABC, and (F) PBS.

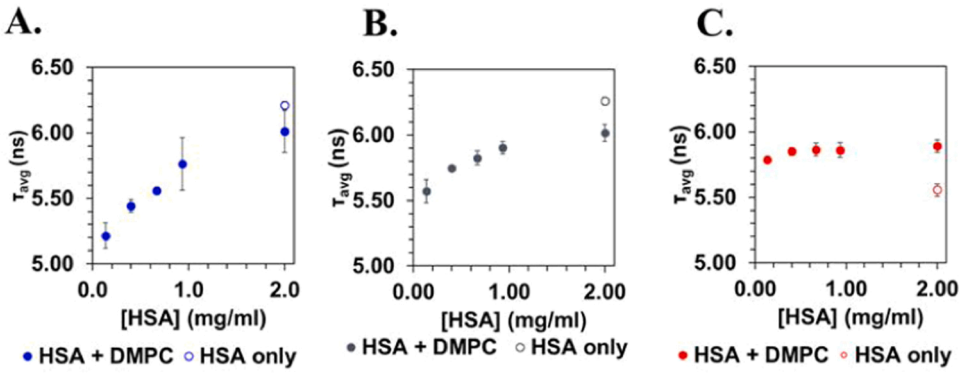


**Fig. 4.** Intensity average lifetime of HSA measured during the interaction with DMPC in: (A) water, (B) ABC, and (C) PBS. The lifetime of free HSA in each buffer is shown by the unfilled markers in each plot.

environment is accompanied by an increase in quantum yield [46]. However, here for water and ABC there was a large decrease in average lifetime (Fig. 4A–B, Table S2, SI) which suggests that HSA partially unfolds, exposing the Trp-214 residue [75,83]. This was observed previously for HSA interaction with DPPC liposomes [84]. In contrast, for PBS, lifetime was nearly constant indicating again that HSA remained in a similar physicochemical environment to the buffer and did not penetrate (Fig. 4C). The small lifetime increase was probably mostly due to reduced rotational mobility on surface binding [46,85,86], but there may also be a contribution from an increased local refractive index [87].

### 3.4. Principal component analysis

PCA (Fig. 5) was first used to identify different interaction mechanisms and assess the degree and type of emission variance. This was done using minimally corrected (i.e., blank subtracted and g-factor corrected) TSFS data (Fig. S13, SI) to also check for outliers, and light scatter effects on sample separation. Three PCs were required in all cases (Table S6, Fig. S14, SI) with PC1 and PC2 typically accounting for ~ 99.8% of the explained variance with PC3 accounting for < 0.1% in all cases. The PCA global model showed that PC1 accounted for ~ 99.2% of variance and was due to increasing HSA emission intensity as the concentration increases. PC2 accounted for ~0.6% of variance and appeared to represent emission spectral shifts. The similar PC1/PC2 trajectories, and high degree of sample spread for water and ABC samples suggested similar types of interaction processes whereas for PBS, there was much less PC2 variance and scatter in the plot which was clear evidence for a different interaction mechanism.

PCA analysis of the sub-models (water, ABC, and PBS, n = 36 each), showed similar loadings and PC1 and PC2 relationship for water and ABC, indicating that they behaved similarly. For PBS, PC2 was insignificant (~0.1%), as no significant spectral shift was present, indicating

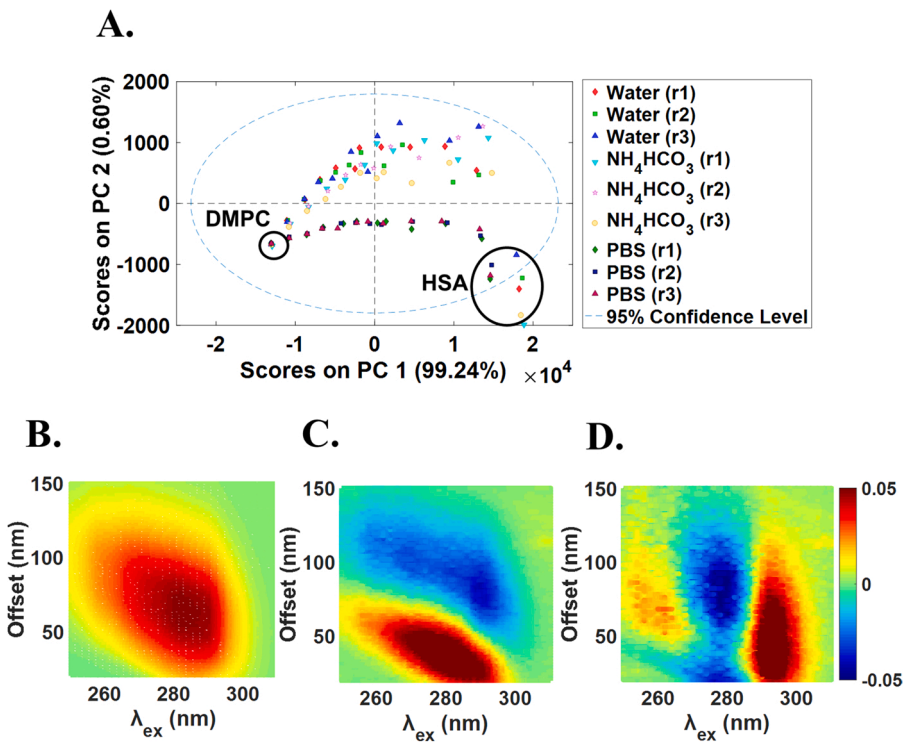


**Fig. 5.** (A) PC1 vs. PC2 scores plots from three component PCA model using t-EEM$_T$ data with all samples (n = 108). Liposome and HSA only samples are circled. The different markers correspond to the replicate measurements for each aqueous medium with markers of the same color corresponding to liposome samples made from a single extrusion. (B–D) Show the PC 1–3 loadings (R-L).

a different, more homogeneous, interaction mechanism (Table S6, Fig. S15/S16, SI). PC3 appeared to be related to Trp emission from three different excitation wavelengths. There was probably more useful information in this component, but the large free HSA emission contribution present prevented accurate interpretation. It was noticeable that minimal scattered excitation light contribution (Fig. S13, SI) was observed in the TSFS$_\perp$ spectra, which confirmed the selected measurement parameters were appropriate for this type of sample and particle size range. However, the effect of increased Mie scatter in the forward direction from ~ 150 nm and greater sized liposome manifests itself by the disappearance of the Raman band in the spectrum of the liposome only samples.

### 3.5. ARMES

Conventional spectroscopic and PCA analysis allowed investigation of the HSA-DMPC interaction using the overall fluorescence emission via shifts in emission and changes in the emission intensity. Anisotropy of the liposome-protein complexes however could not be measured accurately using conventional spectroscopy because of the unbound HSA emission signal and light scattering effects (Fig. 3D–F). However, by using ARMES via PARAFAC analysis, individual emission contributions might be resolved, and anisotropy data could be extracted for the individual components of the fluorescence emission. Intrinsic HSA fluorescence emission comprises of multiple contributions [46,88], and in the presence of liposomes, this becomes more complex with there being three potential HSA species present (free, surface bound, and penetrating) and here we aimed to use PARAFAC to try and resolve these components.

Changes in 3D intrinsic HSA emission with varying HSA/DMPC molar ratios were evaluated in each polarization dataset by PARAFAC. PARAFAC models were created using a global dataset containing all samples, n = 99, (Table S7, SI) and three sub-models were created for water, ABC buffer, and PBS, and the different polarizations, n = 33 for each model (Fig. 6, Table 2). The best models were those using perpendicular polarized spectra as this should be minimally impacted by residual scattered light and thus only be based on fluorescence signal changes. For PBS (Fig. 6C–F), only one PARAFAC component was required (PaC1, $\lambda_{ex/em}$ = 278/352 nm, > 99% explained variance) which correlated with HSA concentration. We contend that this is due to two factors: *1).* that there is no lipid bilayer penetration to generate a large spectral change, and *2).* There was a significant amount of free, unbound HSA present. PARAFAC with this type of data lacked the sensitivity to resolve the very small spectral changes induced by HSA adsorption onto liposome surfaces. A two-component model for PBS was also evaluated (Fig. S19C/F, Table S8, SI) but this was not significantly better than the one component model. However, in the case of water and ABC buffer, PARAFAC recovered two components for each polarization mode (Fig. 6, Table 2). PARAFAC component 1 (PaC1, ~ 42–65% explained variance) appears to correspond to a combination of blue-shifted Trp-214 and tyrosine emission associated with HSA penetration into the lipid bilayer [84]. Component 2 (PaC2, ~ 40–59% explained variance) was related to emission from non-interacting, or surface bound HSA, which shows a more linear relationship with HSA concentration (Table 2, Fig. 6D–E). Plotting the component score ratio versus HSA concentration also shows these different interaction mechanisms (Fig. S18/S20, SI). The high PaC1 scores in water and ABC buffer prove that there is a significant population of interacting HSA, which suggests an end-on interaction based on the requirements for monolayer coverage and the protein-liposome ratios used (Table 1).

t-EEM$_\perp$ measurements appear to be more sensitive towards the interacting HSA population (PaC1) with ~ 11.6–18.0% more variance explained by this component (53 and 60 for water and ABC buffer respectively) compared to 41.5% and 42% for the t-EEM$_\parallel$ model. This is due to two factors, one the better elimination of residual Mie scatter and IFE in the perpendicular polarization measurements, and second, increased HSA emission depolarization upon penetration of the liposome bilayer [10, 89]. One would expect PaC1 scores to reach a

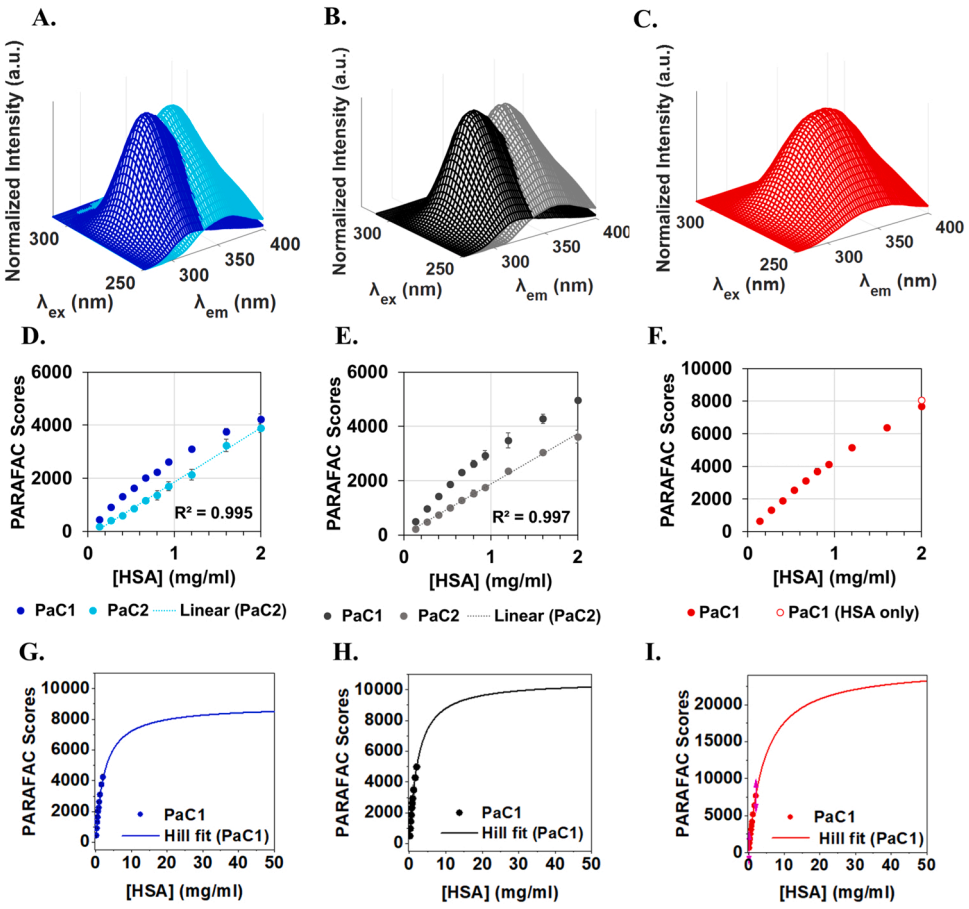


**Fig. 6.** PARAFAC components resolved from sub-models (n = 33) using t-EEM$_\perp$ spectra of: (A) water (2), (B) ABC buffer (2), and (C) PBS (1). Resolved spectra are from a [HSA] = 0.8 mg/ml concentration. PARAFAC scores resolved for PaC1 (and PaC2) in: (D) water, (E) ABC, and (F) PBS. Results of Hill fitting [90] the PaC1 scores in: (G) water, (H) ABC, and (I) PBS. See Fig. S17, SI, for the t-EEM$_T$ model.

**Table 2**
Comparison of model parameters and components obtained for PARAFAC modeling of HSA-liposome samples according to measurement polarization for the buffer specific models (n = 33 in each case).

| Polarization mode | t-EEM$_\parallel$ Water | t-EEM$_\perp$ | t-EEM$_T$ | t-EEM$_\parallel$ ABC buffer | t-EEM$_\perp$ | t-EEM$_T$ | t-EEM$_\parallel$ PBS | t-EEM$_\perp$ | t-EEM$_T$ |
|---|---|---|---|---|---|---|---|---|---|
| PaC1 $\lambda_{ex/em}$ (nm) | 280/320[a] | 280/324 | 278/320 | 280/318[a] | 280/326 | 280/322 | 282/344 | 280/352 | 280/352 |
| PaC1 Fit model (%) | 41.5[a] | 53.1 | 51.9 | 42.6[a] | 60.0 | 65.2 | 100.0 | 100.0 | 100.0 |
| PaC2 $\lambda_{ex/em}$ (nm) | 286/354[a] | 286/358 | 284/358 | 286/358[a] | 284/356 | 282/356 | – | – | – |
| PaC2 Fit model (%) | 58.6[a] | 46.9 | 48.1 | 57.4[a] | 40.0 | 43.1 | – | – | – |
| Variance explained (%) | 99.9 | 99.9 | 100.0 | 99.9 | 100.0 | 99.9 | 99.6 | 99.8 | 99.8 |
| CONCORDIA (%) | 99.2 | 99.9 | 100.0 | 96.1 | 100.0 | 99.9 | 100.0 | 100.0 | 100.0 |
| Split-half analysis (%) | 98.7 | 97.7 | 99.2 | 94.1 | 91.2 | 93.4 | 100.0 | 100.0 | 100.0 |

[a] For these models, the component order was inverted in the model output.

maximum value (at a specific HSA concentration) and then decrease relative to PaC2 scores with increasing HSA concentration if only monolayers were formed. PaC2 scores increased linearly with protein concentration ($r^2 > 0.99$) as expected whereas the PaC1 scores were curved and plateaued at much higher protein concentrations, predicted to be > 30 mg/ml, (Fig. 6G–I). However, at higher HSA concentrations primary IFE becomes more of an issue and thus predicted concentrations are less reliable. For the HSA concentration range used, the correlation between scores and true concentration is also affected by quantum yield, quenching, IFE, and other photophysical processes. As we have seen, both spectral shifts and lifetime changes, so we cannot then use scores to determine accurate concentrations of bound/unbound HSA. That requires further study and purification of protein-liposome complexes and implementation of better IFE correction, unfortunately for intrinsic emission this is not feasible with the protein concentrations used because of high absorbance below 300 nm.

HSA anisotropy at 280/350 nm ($\lambda_{ex/em}$), in all solutions were nearly identical (Fig. 3D–F) and in PBS, PaC1 anisotropy was similar (Fig. S21,

SI), and this was expected because of the unbound HSA obscuring anisotropy changes due to protein adsorption. However, anisotropy calculated from the PARAFAC resolved HSA components in water and ABC, showed significant differences upon interaction with liposomes. PaC1 calculated anisotropies (at the component max emission) were significantly lower (0.08–0.04 in water, 0.09–0.05 in ABC) than the PaC2 values (~0.11–0.13 and ~0.15–0.16) which were higher than for free HSA. Here, PaC1 refers to the bound fraction of HSA (blue shifted emission), and thus the lower anisotropy was not expected. The PaC2 component refers to a mixture of free and surface adsorbed HSA. However, this is a very complex photophysical system and these observations can be explained as arising from multiple factors. First, the large photophysical changes experienced by HSA on incorporation into the bilayer mean that comparing PaC1 anisotropy values with free HSA is not appropriate (they are essentially photophysically and structurally different molecules). Furthermore, changes in Tyr-to-Trp FRET processes will also cause anisotropy changes. Second, radiative energy transfer from PaC1 to PaC2 (particularly since there is excess free HSA) can significantly reduce anisotropy. Third, light losses due to scatter (both primary and secondary) caused by the liposomes will also reduce anisotropy [46]. Finally, secondary scattering IFE (i.e., of the emission) is very different for the parallel and perpendicularly polarized TSFS measurements for this particle size range, making it nearly impossible to extract true anisotropy values in a right-angle measurement geometry [91]. What these component anisotropy values do confirm is that we have resolved two very different populations of HSA species in very different environments. To obtain more accurate intrinsic emission anisotropies requires purification to remove the free HSA contribution, and probably the use of front surface excitation to further reduce the potential for scattered light contamination from the liposomes.

## 4. Conclusions

The experimental goal was to investigate the efficacy of ARMES for better monitoring the changes induced by protein interaction with liposomes in a HSA/DMPC model compared to conventional methods like DLS, absorbance, and fluorescence steady-state and lifetime spectroscopy. ARMES using PARAFAC of HSA intrinsic emission yielded more information about protein-liposome interactions by resolving the different fluorescent components (two different populations of HSA) and their relative contributions to the emission. Two components were extracted for reactions in water and ABC buffer, with component one, showing a large hypsochromic emission shift caused by a combination of lipid bilayer penetration and probably some degree of protein structure modification (making the tryptophan more solvent accessible). The second component with minimal spectral changes more resembled free HSA in solution. In contrast, for PBS, only one component was resolved, and when DLS data were considered, it seems that a non-penetrating protein layer (possibly monolayer) was formed with the adsorbed HSA emission (and thus structure) being similar to that of free HSA in solution. Plotting PARAFAC component score ratios clearly discriminated between the different interaction modes. If the relative quantum yields of both species were known, then one could extract the molar ratio between bound and unbound protein [37]. The PARAFAC recovered component anisotropies were also different, showing that the resolved species were significantly different, however, interpretation of the absolute values is complicated by changing photophysical behavior of the interacting HSA.

In contrast, DLS only reports size changes, and here showed that there were dramatically different interaction mechanisms observed in water, 50 mM ABC, and 10 mM PBS buffer. In water, where there was minimal protein stabilization, liposome disruption by HSA was significant (making DLS measurements unreliable), whereas in ABC and PBS buffers increased protein stabilization meant that interaction led to small, reproducible increases in liposome size and polydispersity. Unfortunately, DLS does not provide any direct information about protein location, and size measurements became unreliable as the particles becomes less monodisperse, making quantitative analysis impossible. Absorbance measurements with MCR data analysis, enabled the resolution of light scatter (from the liposomes) and protein absorption components, and scores plots supported the DLS observations that there were significantly different interaction mechanisms, but gave no explicit protein information except concentration. Conventional lifetime and fluorescence spectroscopy measurements provided information about the changing protein environment, showing clear differences in mechanisms. In water and ABC buffer a significant blue-shift, and lower average lifetime, was measured indicating protein bilayer penetration. In contrast, for PBS no significant blue-shift, and only a small lifetime increase was observed, indicating that HSA remained more in an aqueous like environment. Fluorescence lifetime measurements however requires the use of expensive nanosecond resolution instrumentation which may not be widely available. Using conventional fluorescence anisotropy measurements in this type of sample system with excess free HSA and strongly scattering liposome particles was not feasible [91].

In conclusion, ARMES provides a new way for investigating protein-liposome interactions that exploits the full intrinsic protein emission space and thus avoids the use of extrinsic labels. The use of multivariate data analysis (Fig. S3, SI) provided a comprehensive and structured framework to extract a variety of useful information (resolving different fluorescent species, quantifying their signal contribution, and extracting light scatter signals) all of which can be used to discriminate between interaction mechanisms. With more modern fluorometers that can run absorbance and fluorescence measurements simultaneously [92], implementation of multivariate data analysis could be automated yielding a fast simple measurement, which would facilitate rapid more routine screening of protein-liposome-buffer interactions. Finally, the pTSFS measurements and data analysis procedure can be used to identify the optimal spectral regions which could be used to select simpler 2D measurements for faster in-situ monitoring of interaction kinetics.

To better characterize the protein-liposome complexes at high concentrations where IFE is a big issue, does require removal of the excess free protein and probably the use of front-surface excitation. This would enable more accurate PARAFAC modeling and recovery of more fluorescent components, calculation of correct protein concentrations and anisotropies. Nevertheless, for situations like here where we are comparing different buffers at the same concentration levels, the ARMES method as implemented provides a convenient approach to characterizing different interactions via a comprehensive analysis of the intrinsic protein emission.

## CRediT authorship contribution statement

**Fiona Gordon:** Conceptualization, Designed and performed the experiments, Analysed the data, and wrote the original draft. **Yannick Casamayou-Boucau:** Analysed the data and edited the manuscript. **Alan Ryder:** Conceptualization, Supervision, Funding acquisition, Wrote and edited the manuscript.

## Declaration of Competing Interest

The authors declare that they have no known competing financial interests or personal relationships that could have appeared to influence the work reported in this paper.

## Acknowledgements

This publication has emanated from research supported in part by a research grant from Science Foundation Ireland and is co-funded under the European Regional Development Fund under Grant number (14/IA/2282, *Advanced Analytics for Biological Therapeutic Manufacture*, to AGR). We thank Agilent Technologies (Mulgrave Victoria, Australia) for the

loan of a fluorescence spectrometer. The authors also wish to acknowledge and thank the support of Dr. Steven Quinn from the Physics of Life in the University of York who provided guidance on the preparation of the liposome system used in this studied, his help was a key step in the development of this work.

## Appendix A. Supporting information

Supplementary data associated with this article can be found in the online version at doi:10.1016/j.colsurfb.2021.112310.

## References

[1] A. Akbarzadeh, R. Rezaei-Sadabady, S. Davaran, S.W. Joo, N. Zarghami, Y. Hanifehpour, M. Samiei, M. Kouhi, K. Nejati-Koshki, Liposome: classification, preparation, and applications, Nanoscale Res. Lett. 8 (2013), 102-102.
[2] A.D. Bangham, M.M. Standish, J.C. Watkins, Diffusion of univalent ions across the lamellae of swollen phospholipids, J. Mol. Biol. 13 (1965) 238–252, https://doi.org/10.1016/S0022-2836(65)80093-6, 238-IN227.
[3] M. Li, C. Du, N. Guo, Y. Teng, X. Meng, H. Sun, S. Li, P. Yu, H. Galons, Composition design and medical application of liposomes, Eur. J. Med. Chem. 164 (2019) 640–653.
[4] T. Oberholzer, P.L. Luisi, The use of liposomes for constructing cell models, J. Biol. Phys. 28 (2002) 733–744.
[5] A.D. Bangham, M.W. Hill, N.G.A. Miller, Preparation and use of liposomes as models of biological membranes, in: E.D. Korn (Ed.), Methods in Membrane Biology, 1, Springer, US, Boston, MA, 1974, pp. 1–68.
[6] S.K. Sahoo, V. Labhasetwar, Nanotech approaches to drug delivery and imaging, Drug Discov. Today 8 (2003) 1112–1120.
[7] A. Sharma, U.S. Sharma, Liposomes in drug delivery: progress and limitations, Int. J. Pharm. 154 (1997) 123–140.
[8] L. Sercombe, T. Veerati, F. Moheimani, S.Y. Wu, A.K. Sood, S. Hua, Advances and challenges of liposome assisted drug delivery, Front. Pharmacol. 6 (2015), 286-286.
[9] J.-S. Kim, Liposomal drug delivery system, J. Pharm. Investig. 46 (2016) 387–392.
[10] J. Sabin, G. Prieto, J.M. Ruso, P.V. Messina, F.J. Salgado, M. Nogueira, M. Costas, F. Sarmiento, Interactions between DMPC liposomes and the serum blood proteins HSA and IgG, J. Phys. Chem. B 113 (2009) 1655–1661.
[11] R. Thakur, A. Das, A. Chakraborty, The fate of anticancer drug, ellipticine in DPPC and DMPC liposomes upon interaction with HSA: a photophysical approach, J. Photochem. Photobiol. B 130 (2014) 122–131.
[12] P. Aggarwal, J.B. Hall, C.B. McLeland, M.A. Dobrovolskaia, S.E. McNeil, Nanoparticle interaction with plasma proteins as it relates to particle biodistribution, biocompatibility and therapeutic efficacy, Adv. Drug Deliv. Rev. 61 (2009) 428–437.
[13] F. Bonté, R.L. Juliano, Interactions of liposomes with serum proteins, Chem. Phys. Lipids 40 (1986) 359–372.
[14] S.C. Semple, A. Chonn, P.R. Cullis, Interactions of liposomes and lipid-based carrier systems with blood proteins: relation to clearance behaviour in vivo, Adv. Drug Deliv. Rev. 32 (1998) 3–17.
[15] T. Ishida, H. Harashima, H. Kiwada, Liposome clearance, Biosci. Rep. 22 (2002) 197–224.
[16] W. Yan, L. Huang, The effects of salt on the physicochemical properties and immunogenicity of protein based vaccine formulated in cationic liposome, Int. J. Pharm. 368 (2009) 56–62.
[17] S.K. Kandasamy, R.G. Larson, Effect of salt on the interactions of antimicrobial peptides with zwitterionic lipid bilayers, Biochim. Biophys. Acta 1758 (2006) 1274–1284.
[18] V.S. Stoll, J.S. Blanchard, Buffers: principles and practice, Methods Enzymol. 182 (1990) 24–38.
[19] W. Kunz, J. Henle, B.W. Ninham, 'Zur Lehre von der Wirkung der Salze' (about the science of the effect of salts): Franz Hofmeister's historical papers, Curr. Opin. Colloid Interface Sci. 9 (2004) 19–37.
[20] T.J. Zbacnik, R.E. Holcomb, D.S. Katayama, B.M. Murphy, R.W. Payne, R. C. Coccaro, G.J. Evans, J.E. Matsuura, C.S. Henry, M.C. Manning, Role of buffers in protein formulations, J. Pharm. Sci. 106 (2017) 713–733.
[21] G. Pabst, A. Hodzic, J. Štrancar, S. Danner, M. Rappolt, P. Laggner, Rigidification of neutral lipid bilayers in the presence of salts, Biophys. J. 93 (2007) 2688–2696.
[22] R.A. Böckmann, A. Hac, T. Heimburg, H. Grubmüller, Effect of sodium chloride on a lipid bilayer, Biophys. J. 85 (2003) 1647–1655.
[23] S.K. Kandasamy, R.G. Larson, Effect of salt on the interactions of antimicrobial peptides with zwitterionic lipid bilayers, Biochim. Biophys. Acta 1758 (2006) 1274–1284.
[24] J. Dufourcq, J.-F. Faucon, Intrinsic fluorescence study of lipid-protein interactions in membrane models. Binding of melittin, an amphipathic peptide, to phospholipid vesicles, Biochim. Biophys. Acta (BBA) - Biomembr. 467 (1977) 1–11.
[25] C.A. Kraft, J.L. Garrido, L. Leiva-Vega, G. Romero, Quantitative analysis of protein-lipid interactions using tryptophan fluorescence, Sci. Signal 2 (2009) pl4.
[26] A.S. Ladokhin, Fluorescence spectroscopy in peptide and protein analysis, in: R. A. Meyers (Ed.), Encyclopedia of Analytical Chemistry, John Wiley & Sons Ltd, Chichester, 2000, pp. 5762–5779 (pp).
[27] I.M. Warner, G.D. Christian, E.R. Davidson, J.B. Callis, Analysis of multicomponent fluorescence data, Anal. Chem. 49 (1977) 564–573.
[28] D. Patra, A.K. Mishra, Recent developments in multi-component synchronous fluorescence scan analysis, Trac-Trends Anal. Chem. 21 (2002) 787–798.
[29] B.O. Boateng, S. Elcoroaristizabal, A.G. Ryder, Development of a rapid Polarized Total Synchronous Fluorescence Spectroscopy (pTSFS) method for protein quantification in a model bioreactor broth, Biotechnol. Bioeng. 118 (2021) 1805–1817.
[30] A.L. de Faria e Silva, S. Elcoroaristizabal, A.G. Ryder, Multi-attribute quality screening of immunoglobulin G using polarized Excitation Emission Matrix spectroscopy, Anal. Chim. Acta 1101 (2020) 99–110.
[31] A.L. de Faria e. Silva, S. Elcoroaristizabal, A.G. Ryder, Characterization of lysozyme PEGylation products using polarized excitation-emission matrix spectroscopy, Biotechnol. Bioeng. 117 (2020) 2969–2984.
[32] M. Steiner-Browne, S. Elcoroaristizabal, Y. Casamayou-Boucau, A.G. Ryder, Investigating native state fluorescence emission of Immunoglobulin G using polarized Excitation Emission Matrix (pEEM) spectroscopy and PARAFAC, Chemom. Intell. Lab. Syst. 185 (2019) 1–11, https://doi.org/10.1016/j.chemolab.2018.12.007.
[33] M. Steiner-Browne, S. Elcoroaristizabal, A.G. Ryder, Using polarized Total Synchronous Fluorescence Spectroscopy (pTSFS) with PARAFAC analysis for characterizing intrinsic protein emission, Chemom. Intell. Lab. Syst. 194 (2019), 103871.
[34] F. Gordon, S. Elcoroaristizabal, A.G. Ryder, Modelling Förster resonance energy transfer (FRET) using anisotropy resolved multi-dimensional emission spectroscopy (ARMES), Biochim. Biophys. Acta Gen. Subj. 1865 (2021), 129770.
[35] Y. Casamayou-Boucau, A.G. Ryder, Extended wavelength anisotropy resolved multidimensional emission spectroscopy (ARMES) measurements: better filters, validation standards, and Rayleigh scatter removal methods, Methods Appl. Fluoresc. 5 (2017), 037001.
[36] R.C. Groza, B.Y. Li, A.G. Ryder, Anisotropy resolved multidimensional emission spectroscopy (ARMES): a new tool for protein analysis, Anal. Chim. Acta 886 (2015) 133–142.
[37] Y. Casamayou-Boucau, A.G. Ryder, Accurate anisotropy recovery from fluorophore mixtures using Multivariate Curve Resolution (MCR), Anal. Chim. Acta 1000 (2018) 132–143, https://doi.org/10.1016/j.aca.2017.11.031.
[38] R. Bro, PARAFAC. Tutorial and applications, Chemom. Intell. Lab. Syst. 38 (1997) 149–171.
[39] C.A. Stedmon, S. Markager, R. Bro, Tracing dissolved organic matter in aquatic environments using a new approach to fluorescence spectroscopy, Mar. Chem. 82 (2003) 239–254.
[40] M. Anderson, A. Omri, The effect of different lipid components on the in vitro stability and release kinetics of liposome formulations, Drug Deliv. 11 (2004) 33–39.
[41] V. Weissig. Liposomes, 1 ed., Humana Press, 2010.
[42] M.L. Ferrer, R. Duchowicz, B. Carrasco, J.G. de la Torre, A.U. Acuna, The conformation of serum albumin in solution: a combined phosphorescence depolarization-hydrodynamic modeling study, Biophys. J. 80 (2001) 2422–2430.
[43] M. Gekle, Renal tubule albumin transport, Annu. Rev. Physiol. 67 (2005) 573–594.
[44] A. Tojo, S. Kinugasa, Mechanisms of glomerular albumin filtration and tubular reabsorption, Int. J. Nephrol. 2012 (2012), 481520.
[45] T. Peters, Serum albumin, Adv. Protein Chem. 37 (1985) 161–245.
[46] J.R. Lakowicz, Principles of Fluorescence Spectroscopy, 3rd ed., Springer, New York, 2006.
[47] J. Juan-Colás, L. Dresser, K. Morris, H. Lagadou, R.H. Ward, A. Burns, S. Tear, S. Johnson, M.C. Leake, S.D. Quinn, The mechanism of vesicle solubilization by the detergent sodium dodecyl sulfate, Langmuir 36 (2020) 11499–11507.
[48] P.A. Dalgarno, J. Juan-Colás, G.J. Hedley, L. Piñeiro, M. Novo, C. Perez-Gonzalez, I.D.W. Samuel, M.C. Leake, S. Johnson, W. Al-Soufi, J.C. Penedo, S.D. Quinn, Unveiling the multi-step solubilization mechanism of sub-micron size vesicles by detergents, Sci. Rep. 9 (2019) 12897.
[49] M. Mozafari, E. Mazaheri, K. Dormiani, Simple equations pertaining to the particle number and surface area of metallic, polymeric, lipidic and vesicular nanocarriers, Sci. Pharm. 89 (2021) 15.
[50] B. Valeur, Molecular fluorescence: principles and applications, 2nd Edition ed., John Wiley & Sons, 2002.
[51] J. Jaumot, R. Gargallo, A. de Juan, R. Tauler, A graphical user-friendly interface for MCR-ALS: a new tool for multivariate curve resolution in MATLAB, Chemom. Intell. Lab. Syst. 76 (2005) 101–110.
[52] D.N. Kothawala, K.R. Murphy, C.A. Stedmon, G.A. Weyhenmeyer, L.J. Tranvik, Inner filter correction of dissolved organic matter fluorescence, Limnol. Oceanogr. Methods 11 (2013) 616–630.
[53] H.A.L. Kiers, Hierarchical relations among 3-way methods, Psychometrika 56 (1991) 449–470.
[54] F.L. Hitchcock, The expression of a tensor or a polyadic as a sum of products, J. Math. Phys. 6 (1927) 164–189.
[55] C.J. Carroll, J.D. Analysis, of individual differences in multidimensional scaling via an N-way generalization of an 'Eckart-Young' decomposition, Psychometrika 35 (1970) 283–319.
[56] R.A. Harshman, Foundations of the parafac procedure: model and conditions for an 'explanatory' multi-mode factor analysis, UCLA Work. Pap. Phon, 1970, pp. 1–84.
[57] K. Kumar, A.K. Mishra, Parallel factor (PARAFAC) analysis on total synchronous fluorescence spectroscopy (TSFS) data sets in excitation-emission matrix fluorescence (EEMF) layout: certain practical aspects, Chemom. Intell. Lab. Syst. 147 (2015) 121–130.

[58] K. Matsuzaki, O. Murase, Ki Sugishita, S. Yoneyama, Ky Akada, M. Ueha, A. Nakamura, S. Kobayashi, Optical characterization of liposomes by right angle light scattering and turbidity measurement, Biochim. Biophys. Acta (BBA) - Biomembr. 1467 (2000) 219–226.
[59] L.A. Morton, J.P. Saludes, H. Yin, Constant pressure-controlled extrusion method for the preparation of Nano-sized lipid vesicles, J. Vis. Exp. (2012) 4151.
[60] M. Danaei, M. Dehghankhold, S. Ataei, F. Hasanzadeh Davarani, R. Javanmard, A. Dokhani, S. Khorasani, M.R. Mozafari, Impact of particle size and polydispersity index on the clinical applications of lipidic nanocarrier systems, Pharmaceutics 10 (2018) 57.
[61] H.I. Petrache, S. Tristram-Nagle, D. Harries, N. Kucerka, J.F. Nagle, V.A. Parsegian, Swelling of phospholipids by monovalent salt, J. Lipid Res. 47 (2006) 302–309.
[62] V.A. Parsegian, B.W. Ninham, Application of the Lifshitz theory to the calculation of Van der Waals forces across thin lipid films, Nature 224 (1969) 1197–1198.
[63] N.A. Kim, I.B. An, D.G. Lim, J.Y. Lim, S.Y. Lee, W.S. Shim, N.G. Kang, S.H. Jeong, Effects of pH and buffer concentration on the thermal stability of etanercept using DSC and DLS, Biol. Pharm. Bull. 37 (2014) 808–816.
[64] P. Taboada, S. Barbosa, E. Castro, V. Mosquera, Amyloid fibril formation and other aggregate species formed by human serum albumin association, J. Phys. Chem. B 110 (2006) 20733–20736.
[65] A. Chubarov, A. Spitsyna, O. Krumkacheva, D. Mitin, D. Suvorov, V. Tormyshev, M. Fedin, M.K. Bowman, E. Bagryanskaya, Reversible dimerization of human serum albumin, Molecules 26 (2020).
[66] J. Stetefeld, S.A. McKenna, T.R. Patel, Dynamic light scattering: a practical guide and applications in biomedical sciences, Biophys. Rev. 8 (2016) 409–427.
[67] E. Tomaszewska, K. Soliwoda, K. Kadziola, B. Tkacz-Szczesna, G. Celichowski, M. Cichomski, W. Szmaja, J. Grobelny, Detection limits of DLS and UV-Vis spectroscopy in characterization of polydisperse nanoparticles colloids, J. Nanomater. 2013 (2013), 313081, https://doi.org/10.1155/2013/313081.
[68] Y. Xia, J. Sun, D. Liang, Aggregation, fusion, and leakage of liposomes induced by peptides, Langmuir 30 (2014) 7334–7342.
[69] C. Corbo, R. Molinaro, F. Taraballi, N.E. Toledano Furman, M.B. Sherman, A. Parodi, F. Salvatore, E. Tasciotti, Effects of the protein corona on liposome-liposome and liposome-cell interactions, Int. J. Nanomed. 11 (2016) 3049–3063.
[70] F. Giulimondi, L. Digiacomo, D. Pozzi, S. Palchetti, E. Vulpis, A.L. Capriotti, R. Z. Chiozzi, A. Laganà, H. Amenitsch, L. Masuelli, G. Peruzzi, M. Mahmoudi, I. Screpanti, A. Zingoni, G. Caracciolo, Interplay of protein corona and immune cells controls blood residency of liposomes, Nat. Commun. 10 (2019) 3686.
[71] D.M. Togashi, B. Szczupak, A.G. Ryder, A. Calvet, M. O'Loughlin, Investigating tryptophan quenching of fluorescein fluorescence under protolytic equilibrium, J. Phys. Chem. A 113 (2009) 2757–2767.
[72] V. Džupponová, G. Žoldák, Salt-dependent passive adsorption of IgG1κ-type monoclonal antibodies on hydrophobic microparticles, Biophys. Chem. 275 (2021), 106609.
[73] F. Giulimondi, L. Digiacomo, D. Pozzi, S. Palchetti, E. Vulpis, A.L. Capriotti, R. Z. Chiozzi, A. Laganà, H. Amenitsch, L. Masuelli, G. Peruzzi, M. Mahmoudi, I. Screpanti, A. Zingoni, G. Caracciolo, Interplay of protein corona and immune cells controls blood residency of liposomes, Nat. Comm. 10 (2019) 3686.
[74] S.A. Johnstone, D. Masin, L. Mayer, M.B. Bally, Surface-associated serum proteins inhibit the uptake of phosphatidylserine and poly(ethylene glycol) liposomes by mouse macrophages, Biochim. Biophys. Acta Biomembr. 1513 (2001) 25–37.
[75] B. Christiaens, S. Symoens, S. Verheyden, Y. Engelborghs, A. Joliot, A. Prochiantz, J. Vandekerckhove, M. Rosseneu, B. Vanloo, Tryptophan fluorescence study of the interaction of penetratin peptides with model membranes, Eur. J. Biochem. 269 (2002) 2918–2926.
[76] L.A. Munishkina, A.L. Fink, Fluorescence as a method to reveal structures and membrane-interactions of amyloidogenic proteins, Biochim. Biophys. Acta (BBA) - Biomembr. 1768 (2007) 1862–1885.
[77] C. Sweet, J.E. Zull, Activation of glucose diffusion from egg lecithin liquid crystals by serum albumin, Biochim. Biophys. Acta 173 (1969) 94–103.
[78] S.L. Law, W.Y. Lo, S.H. Pai, G.W. Teh, F.Y. Kou, The adsorption of bovine serum albumin by liposomes, Int. J. Pharm. 32 (1986) 237–241.
[79] R.L. Juliano, H.K. Kimelberg, D. Papahadjopoulos, Synergistic effects of a membrane protein (spectrin) and Ca 2+ on the Na + permeability of phospholipid vesicles, Biochim. Biophys. Acta 241 (1971) 894–905.
[80] K. Hoekstra, J. van Renswoude, R. Tomasini, G. Scherphof, Interaction of phospholipid vesicles with rat hepatocytes: further characterization of vesicle-cell surface interaction; use of serum as a physiological modulator, Membr. Biochem. 4 (1981) 129–147.
[81] L.J. Lis, J.W. Kauffman, D.F. Shriver, Raman spectroscopic detection and examination of the interaction of amino acids, polypeptides and proteins with the phosphatidylcholine lamellar structure, Biochim. Biophys. Acta (BBA) - Biomembr. 436 (1976) 513–522.
[82] C.-M. Lin, D.T. Wu, H.-K. Tsao, Y.-J. Sheng, Membrane properties of swollen vesicles: growth, rupture, and fusion, Soft Matter 8 (2012) 6139–6150.
[83] Y. Chen, M.D. Barkley, Toward understanding tryptophan fluorescence in proteins, Biochemistry 37 (1998) 9976–9982.
[84] R. Thakur, A. Das, A. Chakraborty, Interaction of human serum albumin with liposomes of saturated and unsaturated lipids with different phase transition temperatures: a spectroscopic investigation by membrane probe PRODAN, RSC Adv. 4 (2014) 14335–14347.
[85] D. Toptygin, R.S. Savtchenko, N.D. Meadow, S. Roseman, L. Brand, Effect of the solvent refractive index on the excited-state lifetime of a single tryptophan residue in a protein, J. Phys. Chem. B 106 (2002) 3724–3734.
[86] C.P. Pan, P.L. Muiño, M.D. Barkley, P.R. Callis, Correlation of tryptophan fluorescence spectral shifts and lifetimes arising directly from heterogeneous environment, J. Phys. Chem. B 115 (2011) 3245–3253.
[87] D. Toptygin, R.S. Savtchenko, N.D. Meadow, S. Roseman, L. Brand, Effect of the solvent refractive index on the excited-state lifetime of a single tryptophan residue in a protein, J. Phys. Chem. B 106 (2002) 3724–3734.
[88] A.B.T. Ghisaidoobe, S.J. Chung, Intrinsic tryptophan fluorescence in the detection and analysis of proteins: a focus on forster resonance energy transfer techniques, Int. J. Mol. Sci. 15 (2014) 22518–22538.
[89] D.M. Jameson, J.A. Ross, Fluorescence polarization/anisotropy in diagnostics and imaging, Chem. Rev. 110 (2010) 2685–2708.
[90] R. Gesztelyi, J. Zsuga, A. Kemeny-Beke, B. Varga, B. Juhasz, A. Tosaki, The Hill equation and the origin of quantitative pharmacology, Arch. Hist. Exact. Sci. 66 (2012) 427–438.
[91] M. Ameloot, M. vandeVen, A.U. Acuna, B. Valeur, Fluorescence anisotropy measurements in solution: methods and reference materials (IUPAC Technical Report), Pure Appl. Chem. 85 (2013) 589–608.
[92] A. Quatela, A.M. Gilmore, K.E.S. Gall, M. Sandros, K. Csatorday, A. Siemiarczuk, B. Ben Yang, L. Camenen, A-TEEM (TM), a new molecular fingerprinting technique: simultaneous absorbance-transmission and fluorescence excitation-emission matrix method, Methods Appl. Fluoresc. 6 (2018) 7.